35th Annual International Conference of the IEEE EMBS
Osaka, Japan, 3 - 7 July, 2013

Design of fiber optic applicators for laser interstitial thermotherapy: theoretical evaluation of thermal outcomes

P. Saccomandi, *Student Member, IEEE,* E. Schena, *Member, IEEE* and S. Silvestri, *Member, IEEE*

Abstract— **Thermal effects of different applicators for energy deposition in tissue undergoing laser interstitial thermotherapy (LITT) are investigated. The aim is to predict temperature distribution (*T*), dimensions and shape of thermal lesion produced by the laser light absorption within the tissue, in order to achieve an optimal design of the applicator for LITT. A numerical model, based on Monte Carlo method, was implemented to predict the distribution of laser light within the tissue, and the Bio Heat Equation was used to simulate *T*. Four geometries of optical applicators with different emitting surfaces were considered: bare fiber, cylindrical, zebra and a hybrid geometry. Effects on liver tissue undergoing LITT were evaluated in terms of *T* and coagulation volumes. Simulations were performed with laser power of 3 W and 5 W and energy of 1650 J. Results show that bare fiber causes an irregular coagulation shape; zebra and hybrid applicators 3 cm-long obtain an elliptical lesion, with lowest maximum *T* (*Tmax*) on their surface (about 350 K); cylindrical applicators with length of 1 cm or 1.5 cm produce spherical lesions, with *Tmax* up to 398 K. Results suggest that the selection of the applicator based on the geometry of the lesion could improve LITT outcome. Furthermore, an appropriate geometry can preserve applicator integrity avoiding excessive temperature increase on its surface.**

I. Introduction

LITT is a minimally invasive surgical technique used to destroy tumors by means of laser power delivery that entails temperature increment inside the tissue. The irradiation of tissue by laser light results in the absorption of energy, then converted into thermal energy [1]. The laser light is guided into the organ by an applicator (e.g., optical fiber). The success of therapy depends on both the laser settings (energy, *E*, power, *P*, and treatment time, t) and the applicator for energy deposition.

Because geometry of laser applicator strongly influences the shape and dimensions of the tissue lesion, the goal is to optimize the applicator design, in order to destroy the whole neoplastic mass and to avoid damage to the surrounding healthy tissue.

First applications of LITT employed the applicator called "bare-fiber", i.e., an optical waveguide with an emitting distal end [2]. Its advantages are small diameter (e.g., 300 μm) and affordability, therefore it was extensively used in this field. Biological tissues strongly absorb Nd:YAG laser light, therefore the lesion dimension is quite limited and could be not sufficient for a quick treatment. Besides the employment of multiple applicators [3], a wide and homogeneous initial distribution of the laser light can be achieved by diffusing applicators. Thanks to an appropriate manufacture of their emitting surface, diffusing applicators reduce the power density and the temperature on their surface, and model and control the shape of the tissue to be treated [4]. In all the ablation procedures (e.g., radiofrequency, microwave) efforts are made to design a robust device that can destroy more accurately as possible the whole neoplastic mass, without significant side effects and with predictable outcomes [5].

The present study aims to theoretically investigate the effects of geometry in different typologies of fiber optic applicators on *in vivo* liver tissue, considering both *T* and dimensions of coagulation volume at the end of the procedure. Simulations are performed at two *P* (i.e., 3 W and 5 W) and E=1650 J, according to typical settings of clinical LITT procedures [6, 7, 8].

II. Theoretical Model

A. Photon Propagation Modeling

Monte Carlo simulation can be employed for modeling the phenomenon of photons emission from the applicator surface and, consequently, propagation through a biological medium. Initially, a weight (*w*) equal to 1 is assigned to each photon. N photons are set into the tissue at a certain location, depending on the geometry and shape of the applicator, defined by *x, y, z* coordinates. Their trajectory is specified by the directional cosines (u_x, u_y, u_z), corresponding to the trajectories projection onto the corresponding axes. The random distance, traveled before the photon interacts with the tissue, depends on a random number ranging from 0 and 1, and on the total attenuation coefficient $\mu_t=\mu_a+\mu_s$, where μ_a and μ_s are the absorption and scattering coefficient of the tissue, respectively. After each photon step, *w* is reduced by absorption, and the remaining non-absorbed *w* is redirected according to a phase function, that describes the angular dependence of a single scattering. Once a new trajectory is defined, the photon is again moved on through the tissue. During the propagation, *w* drops until it reaches a threshold value, typically chosen as 10^{-4} [1].

The tissue is modeled as a 3D grid of bins, each indexed with *ix*, *iy*, *iz*, according to the three spatial coordinates. The volume of each bin is V [cm^3]. The length of photon step, s [cm], is exponentially distributed, as expressed by the probability, *p(s)*, in (1)

This work has been carried out under the financial support of Filas-Regione Lazio in the framework of the ITINERIS2 project (CUP code F87G10000120009).

P. Saccomandi, E. Schena and S. Silvestri are with the Unit of Measurements and Biomedical Instrumentation, Center for Integrated Research, Università Campus Bio-Medico di Roma, Via Álvaro del Portillo, 21-00128-Rome-Italy.

$$p(s) = \frac{\exp(-\mu_t \cdot s)}{\mu_t} \quad (1)$$

By the integration of $p(s)$, evaluated at a particular s_1, the probability distribution function $F(s_1)$ is defined from (1):

$$F(s_1) = \int_0^{s_1} p(s)ds = 1 - \exp(-\mu_t \cdot s_1) \quad (2)$$

A random number rnd_1 is equal to $F(s_1)$, according to:

$$rnd_1 = F(s_1) = 1 - \exp(-\mu_t \cdot s_1) \quad (3)$$

From (3) we obtain:

$$s_1 = \frac{-\ln(rnd_1)}{\mu_t} \quad (4)$$

The position and trajectory of each photon at i-step of simulation is defined as follows:

$$\begin{cases} x_{i+1} = x_i + s \cdot u_{xi} \\ y_{i+1} = y_i + s \cdot u_{yi} \\ z_{i+1} = z_i + s \cdot u_{zi} \end{cases} \quad (5)$$

At each step, the photon is scattered into a new trajectory according to two scattering functions, used to establish the angles of scattering θ (defined by the Henyey-Greenstein phase function [1]) and φ, respectively the deflection and azimuthal scattering angles:

$$\begin{cases} \theta = \arccos\left\{ \frac{1}{2g} \cdot \left[1 + g^2 - \left(\frac{1 - g^2}{1 - g + 2g \cdot rnd} \right)^2 \right] \right\} \\ \varphi = 2\pi \cdot rnd \end{cases} \quad (6)$$

At each step, the photon interacts with the tissue: a fraction $w \cdot (\mu_a/\mu_t)$ is absorbed by the tissue, whereas the remaining one, $w \cdot (\mu_s/\mu_t)$, keeps on propagating. The absorption process is described as follows:

$$A_{i+1} = A_i + w_i \cdot \frac{\mu_a}{\mu_t} \quad (7)$$

where A is the matrix that stores the absorption contribution of each photon, at each step. It is possible to define the fluence rate ψ, [W·cm^{-2}] :

$$\Psi = P \cdot M \quad (8)$$

where P is the power emitted by the laser source, and

$$M = \frac{A}{V \cdot N \cdot \mu_a} \quad (9)$$

In the implementation of this model, the following variable values have been selected: N=10^5, μ_a= 0.24 cm^{-1}; μ_s=300 cm^{-1}, g =0.95 (liver tissue).

B. Thermal Model

Photons absorption within the tissue entails a temperature increase, that can be estimated by the Bio Heat Equation [6-9]:

$$\rho \cdot c \frac{\partial T(x,y,z,t)}{\partial t} = \nabla(k \nabla T(x,y,z,t)) + Q_s + Q_b + Q_m - Q_e \quad (10)$$

where ρ=1050 kg·m^{-3} is liver density, c=3600 J·kg^{-1}·K^{-1} is the liver specific heat and k=0.5 W·m^{-1}·K^{-1} is the liver heat conductivity [8]. $T(x,y,z,t)$ is the tissue temperature as a function of spatial coordinates x, y, z and time, t. Tissue is assumed homogeneous and isotropic to make the heat transfer analysis more feasible and to maintain generality.

Other terms in (10) are:

- Q_s [W·m^{-3}], the heat source specific power:

$$Q_s = \mu_a \cdot \Psi \quad (11)$$

- Q_b [W·m^{-3}], the heat absorption due to blood perfusion per volume unit in the tissue:

$$Q_b = \rho_b \cdot c_b \cdot w_b (T(x,y,z,t) - T_b) \quad (12)$$

where ρ_b=1060 kg·m^{-3} is the blood density, c_b=3640 J·kg^{-1}·K^{-1} is the blood specific heat, w_b=0.0253 s^{-1} is the blood perfusion rate per volume unit [s^{-1}] and T_b the blood temperature outside the treatment region [9];

- Q_m [W·m^{-3}], the metabolic heat generation per unit of volume, due to oxidative process of lipids, proteins and carbohydrates, considered equal to 33800 W·m^{-3} [9];

- Q_e [W·m^{-3}] is the power absorption due to water evaporation [9].

Two simulation environments were utilized: the Monte Carlo model for photon propagation through tissue was implemented in Matlab 2010a, whereas the thermal model based on Bio Heat Equation was simulated in Comsol Multiphysics 3.5a.

Figure 1 reports the flowchart of simulation including the main blocks (i.e., Monte Carlo modeling and Bio Heat Equation), and the respective input variables (i.e., applicator characteristics, optical and physical properties of tissue) and outputs (fluence rate and tissue temperature distribution).

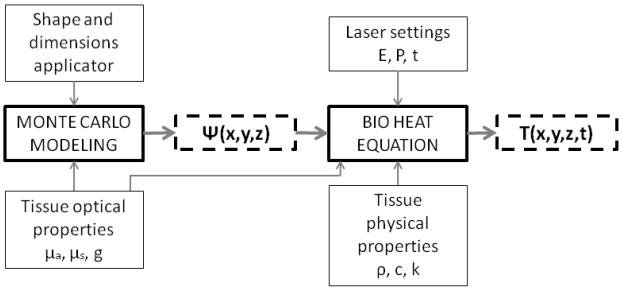

Figure 1. Flowchart of simulation.

III. Results and Discussion

This section reports the results of numerical simulations, distinguished between fluence rate and temperature distribution graphs.

A. Fluence Rate Distribution

The initial position and direction of photons is specified for each typology of applicator (Table I):

TABLE I. INITIAL POSITION AND DIRECTION

	Bare fiber	Cylindrical applicator	Zebra applicator	Hybrid applicator
	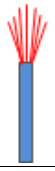	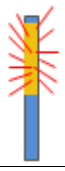	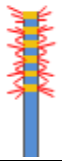	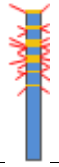
x_{in}	$\sigma\sqrt{-ln(rand)}$	$r_a \cdot cos(t)$	$r_a \cdot cos(t)$	$r_a \cdot cos(t)$
y_{in}	$\sigma\sqrt{-ln(rand)}$	$r_a \cdot sin(t)$	$r_a \cdot sin(t)$	$r_a \cdot sin(t)$
z_{in}	1	2+rand	$z=1+3 \cdot rand$ 10 emitting regions, each of length 1.5 mm, and equidistant (1.5 mm)	$z=1+3 \cdot rand$ 6 emitting regions with growing surface when directed to the applicator centre, and equidistant (1.5 mm)
ux_{in}	0	$cos(t) \cdot cos(\varphi)$	$cos(t) \cdot cos(\varphi)$	$cos(t) \cdot cos(\varphi)$
uy_{in}	0	$cos(t) \cdot sin(\varphi)$	$cos(t) \cdot sin(\varphi)$	$cos(t) \cdot sin(\varphi)$
uz_{in}	1	$cos(t)$	$cos(t)$	$cos(t)$

-r_a: applicator radius [cm]
-t=arcos(rand), where rand is a randomic value obtained from the standard uniform distribution on the open interval (0,1)
-Bare fiber initial position is explained in Appendix A

The random number is used in the definition of initial position when photons are launched from a surface (Table I). In zebra and hybrid applicators, emitting regions are spaced out with non-emitting ones, in order to decrement ψ.

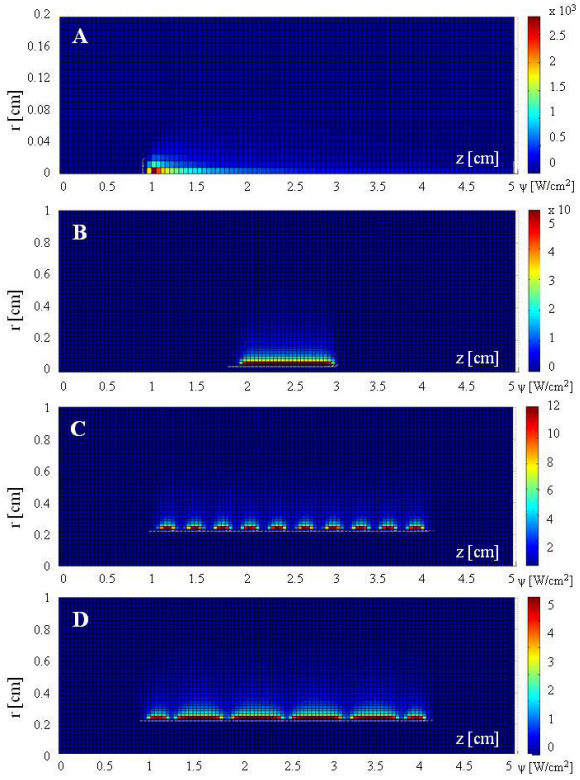

Figure 2. Images of fluence rate, ψ [W/cm^2] for A) bare fiber, B) cylindrical 1 cm-long, C) zebra and D) hybrid applicator.

Figure 2 shows the distribution of ψ inside the tissue. Thanks to the cylindrical symmetry of the geometry, ψ is plotted in the r, z plane. As expected, ψ distribution varies with the geometry of the applicator: in particular, the highest ψ is obtained with a bare fiber (fig. 2A), with a maximum value of $3 \cdot 10^3$ W·cm^{-2}, it decreases in cylindrical and zebra applicator (50 W·cm^{-2} and 12 W·cm^{-2}, respectively), and in hybrid applicator (about 5 W·cm^{-2}). This behavior is mainly due to the size of the emitting surface: in fact, the bare fiber emits N photons from its tip (diameter of 300 µm and surface of $7 \cdot 10^{-4}$ cm^2), where they are extremely concentrate, whereas in other applicators the emission surface increases, and, consequently, ψ decreases.

B. Thermal Distribution

Temperature distribution inside the tissue is obtained by solving (9). *E* was set at 1650 J and *P* was set at 3 W and 5 W. Results for *P*=3 W are shown in fig. 3.

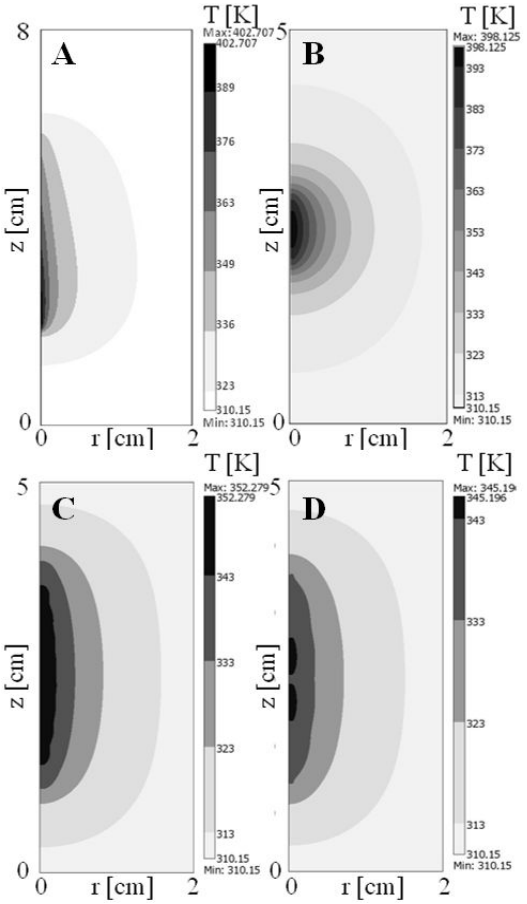

Figure 3. Temperature distribution at the end of LITT (*P*=3 W) produced by A) bare fiber, B) cylindrical 1 cm-long, C) zebra and D) hybrid applicator.

Maximum *T* (*Tmax*) decreases from about 400 K for bare fiber and cylindrical applicator, to about 350 K for zebra and hybrid applicators. Besides the temperature distribution, the comparison of thermal effects of different applicators can be obtained by considering the isothermal surface at 333 K (60 °C). As a matter of fact, thermal injury in a living tissue undergoing LITT depends on *T* reached during treatment and application time. As introduced by McKenzie [10], the

tissue coagulation threshold is about 60 °C, that corresponds to the protein denaturation and coagulation of vessels; therefore, the visualization of the region of coagulation allows to compare the thermal effects of proposed applicators.

Figure 4 shows the thermal damage ($T \geq 60$ °C) for the applicators, at 3 W and 5 W. The effects of cylindrical applicator were simulated for length of diffusing surface of: 1 cm (fig. 4D), 1.5 cm (fig. 4E) and 3 cm (fig. 4F).

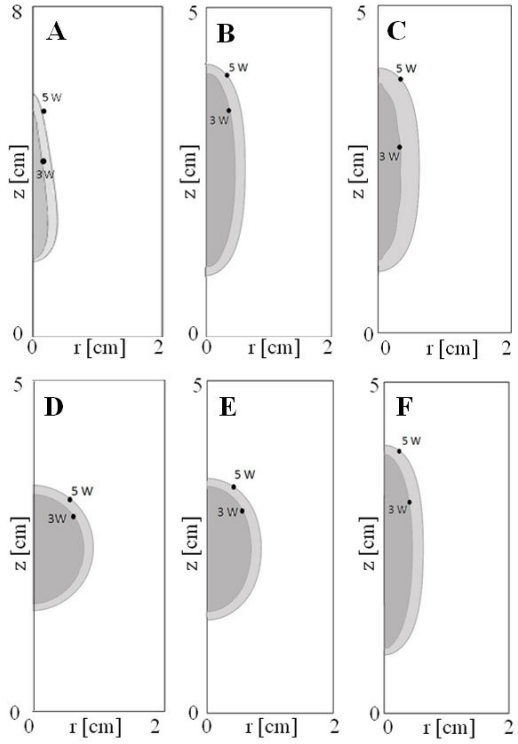

Figure 4. Temperature distribution at the end of LITT (P=3 W and P=5 W) produced by A) bare fiber, B) zebra applicator, C) hybrid applicator, and cylindrical applicator D)1 cm, E) 1.5 cm and F) 3 cm-long.

Bare fiber causes an irregular coagulation shape (fig. 4A); zebra applicator 3 cm-long (fig. 4B), hybrid (fig. 4C) and cylindrical ones (fig. 4F) produce a similar damage region, both in volumes (at 5 W it ranges between 4 cm^3 and 5 cm^3) and in shape (ellipsoid), although the *Tmax* reached on the applicator surface is slightly different (fig. 3C and 3D). Cylindrical applicators with diffusing length of 1 cm (fig. 4D) and 1.5 cm (fig. 4E) obtain almost spherical volumes of damage, of about 3.5 cm^3 and 6 cm^3 at 5 W, respectively. Also, Ahrar *et al.* [11] employed a water-cooled applicator with diffusing surface of 1 cm, that although different laser settings and the drawback of the composed system, obtain similar results, in term of spherical shape of thermal damage. Benefit of a spherical lesion is the temperature distribution inside the tissue, that allows to easily perform a controlled and predictable amount of tissue removal. Furthermore, applicators with spaced out emitting regions entail low T on their surface, and preserve themselves.

IV. Conclusions

Numerical evaluation of thermal effects of different typologies of applicators for LITT is useful to predict temperature on applicator surface, and shape and dimensions of tissue volumes to be removed. First of all, estimation of surface temperature is valuable to preserve the integrity of applicator during the treatment. Furthermore, simulations show that geometry of applicator strongly influences dimensions and shape of lesion. Therefore, this evaluation is crucial for driving the clinician in the optimal choice of the suitable applicator and the effective laser settings, depending on the morphology of the tumor to be treated.

Appendix A

Considering that the laser beam guided by a bare fiber can be described with a Gaussian distribution, the probability density function of the radial position of launch is:

$$p(r) = \frac{\exp\left(-r^2/\sigma^2\right)\cdot 2\pi r}{\pi\sigma^2} \qquad (12)$$

and the respective probability distribution function is:

$$F(r_1) = \int_0^{r_1} p(r)dr = \exp(-r_1^{\,2}/\sigma^2) \qquad (13)$$

According to the Monte Carlo method, we obtain:

$$r_1 = \sigma\sqrt{-\ln(rand)} \qquad (14)$$

References

[1] A. J. Welch and M. J. C. van Gemert, "Optical-Thermal Response of Laser-Irradiated Tissue," 2th edition, *Springer*, 2011, pp. 42-56.

[2] C. M. Philipp, E. Rhode and H. P. Berlien, "Nd:YAG laser procedures in tumor treatment," *Semin Surg Oncol*, vol. 11, no. 4, pp. 290-298, Jul. 1995.

[3] L. M. Veenendaal, A. de Jager, G. Stapper, I. H. Borel Rinkes and R. van Hillegersberg, "Multiple fiber laser-induced thermotherapy for ablation of large intrahepatic tumors," *Photomed Laser Surg,* vol. 24, pp. 3-9, 2006.

[4] H. J. Schwarzmaier et al, "Improved laser applicators for interstitial thermotherapy of brain structures," *Society of Photo-Optical Instrumentation Engineers (SPIE), v*ol. 2132, pp. 4-12, May 1994.

[5] A. P O'Rourke, D. Haemmerich, P. Prakash, M. C. Converse, D. M. Mahvi, and J. G. Webster, "Current status of liver tumor ablation devices," *Expert Rev Med Devic*, vol. 4, no. 4, pp. 523-537, 2007.

[6] P. Saccomandi et al., "Laser Interstitial Thermotherapy for pancreatic tumor ablation: theoretical model and experimental validation," in *Proc. 33rd Annu. International Conf. IEEE Eng Med Biol Soc*, Boston, 2011, pp. 5585-5588.

[7] P. Saccomandi et al., "Theoretical assessment of principal factors influencing laser interstitial thermotherapy outcomes on pancreas," *Proc. 34rd Annu. International Conf. IEEE Eng Med Biol Soc*, San Diego, 2012, pp. 5687-5690.

[8] G. Müller and A. Roggan, "Laser-induced interstitial thermotherapy," SPIE Press , 1995.

[9] P. Saccomandi, E. Schena, M. A. Caponero, F. M. Di Matteo, M. Martino, M. Pandolfi and S. Silvestri, "Theoretical analysis and experimental evaluation of laser induced interstitial thermotherapy in ex vivo porcine pancreas," *IEEE T Bio-Med Eng*, vol. 59, no. 10, pp. 2958-2964, Oct. 2012.

[10] A. L. McKenzie, "Physics of thermal processes in laser-tissue interaction," *Phys Med Biol*, vol. 35, no. 9, pp. 1175-1209, Sep. 1990.

[11] K. Ahrar, et al, "Preclinical assessment of a 980-nm diode laser ablation system in a large animal tumor model," *J Vasc Interv Radiol*, vol. 21, no. 4, pp. 555-561, 2010.